https://doi.org/10.5194/egusphere-2025-2843
Preprint. Discussion started: 28 July 2025

Baseflow in karst regions is significantly higher than the global average and exhibits spatial variability

Author :Ze Yuan [a,b], Qiuwen Zhou [a,b]*, Yuan Li [a,b]*, Yuluan Zhao [a,b], Shengtian Yang [c,d]
Affiliation:
a. School of Geography and Environmental Science, Guizhou Normal University, 550001 Guiyang, China
b. Karst Ecosystem Field Scientific Observation and Research Station of Guizhou Normal University & Guanling Autonomous County, 561300 Guanling, China
c. Institute of Ecological Civilization, Guizhou Normal University, 550001 Guiyang, China
d. College of Water Sciences, Beijing Normal University, 100875 Beijing, China
Corresponding author: Qiuwen Zhou *, Yuan Li*
Email: zqw@gznu.edu.cn, Yuan Li: liyuan7pro@163.com

https://doi.org/10.5194/egusphere-2025-2843
Preprint. Discussion started: 28 July 2025

Abstract: The distinct hydrogeological configurations of karst terrains engender fundamentally divergent baseflow regimes compared with non-karst systems. However, there is still some uncertainty in the understanding of baseflow in global karst regions due to the variability of methods and differences in natural conditions in different regions. In this study, runoff data from 1375 karst basins around the world were summarized, and graphical and digital filtering methods were used to estimate baseflow in global karst regions and to analyze their spatial differences and trends. The results show that the baseflow index of global karst areas is about 78 ± 6.9%, which is significantly higher than the global average baseflow index (60%). The baseflow index of karst regions in different climatic zones also differed significantly, in which the average baseflow index of arid karst regions (82%) was significantly higher than the average baseflow index of subtropical karst regions (77%). Even within the same climate zone, the base flow index of different regions may also have significant differences, and the difference of some regions is even >10%. Vegetation factors reflected in primary productivity have the highest influence on baseflow in karst regions (15%), while climatic factors (relative humidity, air temperature, etc.) have a lower influence on BFIs in karst regions (less than 5%). From the time series trend, the global karst baseflow index shows an increasing trend, about 1.5% from 1960 to 2015. These results help us to further understand karst hydrological processes and the response mechanism of karst hydrology under climate change.

Key words: Baseflow; Karst; Hydrographic graphical method; climate zone; global runoff data; hydrogeology

https://doi.org/10.5194/egusphere-2025-2843
Preprint. Discussion started: 28 July 2025

1. Introduction

Baseflow plays a central role as a slow recharge component of groundwater to runoff as a hydrological stabiliser (Mukherjee et al., 2018; Chen et al.,2019). The proportion and dynamic characteristics of baseflow in runoff not only regulate the ecological balance threshold of rivers, but also profoundly affect the resilience of watersheds in response to climate fluctuations (Saedi et al ., 2022; Hare et al., 2021; Yang et al., 2023). Therefore, accurate quantification of the characteristics of baseflow can help to understand the runoff evolution pattern and its response mechanism to regional environmental changes (Mei et al., 2024; Kuehne et al., 2023).

Recent studies on baseflow estimation have revealed its spatial variability characteristics. Among them, Xie et al (2023), based on a coupled analysis of baseflow separation and climate models for 15,000 catchments worldwide, pointed out that the average contribution of baseflow to river runoff was about 60%. However, there are significant regional differences under this macroscopic pattern, e.g., baseflow index (BFI) calculations by Beck et al (2013) for 3,394 watersheds globally show that BFI is generally higher in tropical and temperate-cold regions than in arid and semi-arid zones (e.g., North and South Africa, Central Asia, and Australia). Regional scale studies further refine the spatial differentiation pattern, such as the United States, where the BFI is higher in the east than in the west, India, where the BFI is higher in the east than in the west, and the Yellow River basin, where it is higher in the upstream and downstream and lower in the middle reaches, whereas the BFI of the Wei River basin in the Loess Plateau shows a gradual decrease from the upstream to the downstream (Mei et al ., 2024 ; Sharma and Mujumdar ., 2024 ; Lyu et al ., 2023 ; Zhang et al ., 2019).

The current study characterises global baseflow features, but the unique hydrological structure of karst landscapes (e.g., pipes and fissures) makes the baseflow features obtained from the above study significantly less applicable in karst regions (Jiang et al., 2024 ; Ford & Williams, 2007). The current study found significant regional differences in BFI characteristics in karst regions around the world. In particular, the high permeability of karst media in tropical karst regions (e.g., Sumatra, Java) contributes to the rapid conversion of precipitation to groundwater, as analysed in three sub-basins of the Brantas Hulu watershed, where the BFI exceeds 80% (Pratama and Adji., 2020), and the study of three basins in Jonggrangan area also showed BFI of more than 87 per cent (Khomsiati et al., 2021). Seasonal differences in

https://doi.org/10.5194/egusphere-2025-2843
Preprint. Discussion started: 28 July 2025

BFI are highlighted in subtropical karst regions (Mediterranean Sea, Southern China), such as central Italian basins with baseflow contributions spanning 30-76%, rising to 88-90% in dry months (Longobardi and Loon., 2017), and southeastern France has significant differences in baseflow contributions (27%-61%) in years of abundant and dry water (Guisiano et al., 2024). Temperate karst regions such as the Sierra Nevada karst region in North America generally have BFI higher than 65% (Tobin and Schwartz., 2019). The BFI in the karst region of southwest China is 57% (Mo et al., 2025), a stable BFI of ⩾55% in temperate karst in central Ireland (Foran et al., 2021), and a BFI of 36±10% in the karst mountains of eastern China (Lyu et al., 2022).

In summary, studies of baseflow in karst regions have revealed their obvious spatial heterogeneity. A large number of studies have characterised the baseflow characteristics of karst under different climatic zones, and also outlined the regional baseflow characteristics of karst under different climatic zones (Tagne and Dowling., 2018). However, existing studies still have obvious limitations, starting with an over-focus on localised features in small regions, such as watershed studies in southern China and the Mediterranean (Guisiano et al., 2024; Mo and Ruan., 2021), which makes the results of the study not necessarily representative of the global karst region. The second is the variability of research methods, such as hydrographic methods (graphical methods, digital filtering methods), isotope tracer methods, etc. (He et al., 2019; Yang et al ., 2021 ; Arnold et al.,2013). The difference in focus of the different methods also reduces the commonality of the findings. These two reasons have led to a lack of characterisation of overall features and reasonable quantification of regional differences, despite the exploration of baseflow characteristics of karst basins in different regions of the world (Wu et al., 2017; Mei et al., 2024). Therefore, the complete characterisation of baseflow in the global karst region using reasonable methods and the accurate quantification of the overall characteristics and regional differences of baseflow in the global karst region are still urgently needed.

The aim of this study is to explore the baseflow characteristics and their internal differences in the global karst region and to discuss the influence of different factors on baseflow in karst regions. Global public runoff data were selected for the study, and daily-scale runoff data from 1375 watersheds within the karst region were selected. Twelve baseflow separation methods, including four graphical methods and eight digital filtering methods, were used to separate the baseflow from the runoff data and calculate BFIs. The reliability of the results was assessed using the Kling-Gupta

https://doi.org/10.5194/egusphere-2025-2843
Preprint. Discussion started: 28 July 2025

Efficiency (KGE) (Gupta et al., 2009) and Nash-Sutcliffe Efficiency (NSE) (Nash and Sutcliffe., 1970) coefficients, and finally, the XGBoost model was used to analyse the influencing factors of the 12 indices on baseflow.

2. Materials and methods

2.1 Data sources

2.1.1 Runoff data

We have selected regions with a concentrated distribution of karst landscapes worldwide. And combined with global watershed data (Lehner and Grill, 2013), Köppen climate zoning, and urban distribution, select runoff observation stations with less human activity and watershed areas less than 2500 km^2. Thus daily runoff data for 1412 watersheds with different time spans have been selected. The runoff data mainly comes from the Global Runoff Data Center (https://www.bafg.de/GRDC), The European Water Archive (https://ne-friend.bafg.de/servlet/), National River Flow Archive, UK (https://nrfaapps.ceh.ac.uk/nrfa/nrfa-api.html), Brazilian National Water Authority (https://zenodo.org), The National Hydrological Data Archive of Canada (https://wateroffice.ec.gc.ca/), The Chinese Ministry of Water Resources (http://www.cjh.com.cn/), The National Hydrological Information System of the United States (https://waterdata.usgs.gov/nwis).

Due to quality differences in data from different hydrological observation stations, it is necessary to clean the data from these 1412 stations. Exclude sites with severe data gaps and supplement data from sites with a small amount of missing data. We use cubic spline interpolation and linear interpolation to supplement data with missing amounts less than 30 days. Finally, daily runoff data of 1375 watersheds in different time ranges of karst regions worldwide were obtained. This includes 221 watersheds in tropical karst zones, 91 watersheds in arid karst zones, 490 watersheds in subtropical karst zones, and 568 watersheds in temperate karst zones (Figure 1).

https://doi.org/10.5194/egusphere-2025-2843
Preprint. Discussion started: 28 July 2025

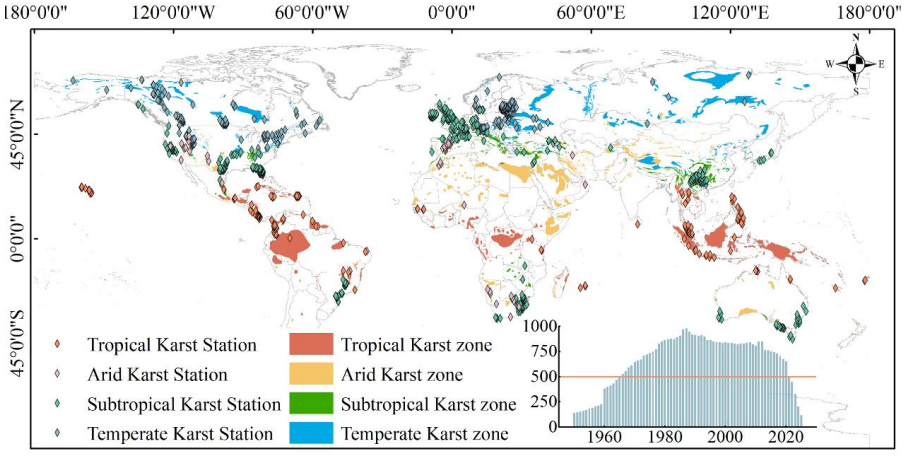

Figure 1. The distribution of karst landscapes and hydrological stations in various climate zones around the world. The bar chart represents the number of hydrological stations selected in each year, with the vertical axis indicating the number of selected hydrological stations and the horizontal axis indicating the year. We selected years with over 500 hydrological stations that meet the requirements within the same year for subsequent analysis.

2.1.2 Selection of potential influencing factors of base flow

In order to analyse the influencing factors of baseflow, we further selected daily-scale runoff data from 744 hydrological stations during 2011-2012 out of the 1375 hydrological stations mentioned earlier to calculate baseflow. The purpose of further selecting the hydrological stations is to ensure the continuity of the data while at the same time ensuring that the stations can cover the major karst regions of the world. We selected a total of 12 potential influences. Climatic factors included temperature and rainfall, and geological factors included depth to bedrock, water storage in epikarst, slope, elevation, and soil evaporation. Other factors included runoff, population density, gross primary productivity (GPP), relative humidity, and surface radiation, for a total of 12 factors (Table 1).

Table 1. Detailed information on the 12 influencing factors

Name	Temporal scale	Spatial resolution	Data sources
Runoff volume	Monthly everage	-	The same as the runoff data in Section 2.1.1
Epikarst water storage volume	Monthly everage	30 arc-second	GES(Goddard Earth Sciences)DISC(Li et al .,2019)
Bedrock depth	-	0.25km×0.25 km	ISRIC — World Soil Information (Hengl et al .,2017)

https://doi.org/10.5194/egusphere-2025-2843
Preprint. Discussion started: 28 July 2025

Air temperature	Monthly everage	30 arc-second	Climatic Research Unit gridded Time Series(arris et al .,2020)
Precipitation	Monthly everage	30 arc-second	
Relative humidity	Monthly everage	0.1°×0.1°	
Elevation	-	30 arc-second	Worldclim(Fick and Hijmans .,2017)
Slope stepness	-	30 arc-second	
Available soil moisture	multi-year average	1km×1km	HWSD(Harmonized World Soil Database)(Wieder et al .,2014)
Population density	multi-year average	30 arc-second	LandScan Global 30 Arcsecond Annual Global Gridded Population Datasets (Bright et al., 2013)
Gross primary production	multi-year average	0.25°×0.25°	TU Data Repository(Wild et al.,2022)
Land-surface radiation	Monthly everage	10km	Data Center of the Qinghai-Tibet Plateau(Tang .,2019)

2.2 Methods

2.2.1 Baseflow separation methods

Commonly used methods for baseflow separation include isotope tracer methods, hydrological modelling methods and hydrographic methods (including graphical methods and digital filtering methods). However, the isotope tracer method relies on high-precision isotope data and is difficult to be extended in data-poor areas, while the hydrological modelling method is limited by the empirical nature of the parameters as well as the regional nature. Therefore, considering the characteristics of the study area (wide range and insufficient observational data), we chose the hydrographic method, which requires less data and is relatively simple.

The computational tool used for baseflow separation in this study is from the Python library baseflow (https://pypi.org/project/baseflow) developed by the team of Xiaomang Liu at the Chinese Academy of Sciences, which contains four graphical methods and eight digital filtering methods that allow simultaneous implementation of multiple methods for baseflow separation (Xie et al. 2024). In addition to this the baseflow library evaluates each method when separating the baseflow and obtains an optimal method. In this study, the baseflow library was used to separate baseflow from global runoff data and calculate its multi-year average BFI (Figure 6).

Graphical methods are techniques for isolating baseflow by analysing runoff hydro-graph. The four graphical methods used in this study are Fixed Interval Method

https://doi.org/10.5194/egusphere-2025-2843
Preprint. Discussion started: 28 July 2025

(FIM), Local Minimum Method (LMM), Sliding Window Method (SW) and UK Institute of Hydrology (UKIH).

Digital filtering is a baseflow segmentation method that uses digital signal processing techniques to separate baseflow from runoff by designing specific filters. These methods usually involve one or two parameters, such as the recession coefficient. The recession constant is automatically estimated in the baseflow library using the Brutsaert method, and the second parameter is calibrated using the multi-objective optimisation method proposed by Arnold (Brutsaert., 2008; Rammal et al., 2018). The methods used in this work include the Boughton Method (Boughton), Chapman-Maxwell Filter Method (CM), Chapman Filter Method (Chapman), Exponential Weighted Moving Average (EWMA), Eckhardt Filter Method (Eckhardt), Furey Digital Filter Method (Furey), Lyne-Hollick Digital Filter Method (LH), and Willems Digital Filter Method (Willems).

2.2.2 Evaluation metrics for baseflow separation methods

In order to validate the accuracy of different baseflow separation methods in karstic regions, we chose two metrics, KGE and NSE coefficients, to measure the effectiveness of different methods in separating baseflows. The methodology used by Xie et al (2020) for measuring and assessing the effectiveness of baseflow separation methods in the US region was used, which centred on screening for strict baseflow points.

2.2.3 Attributional analysis methods

Due to the significant differences in magnitude of the potential influences selected at the global scale (a few hydrological stations are at extremely high elevations, whose actual differences are compressed after normalisation, making it difficult to adequately characterise the effect of elevation on baseflow), traditional linear models or distance metric-based algorithms are susceptible to magnitude interference. Therefore, we chose the magnitude-insensitive XGBoost model, which naturally circumvents the feature scale difference problem through the splitting rule of the tree structure (Niazkar et al.,2024; Zhang et al., 2022). In addition, the model's built-in regularisation mechanism and subsampling strategy can effectively suppress overfitting and guarantee the model's generalisation ability in complex geographic data. The model also supports parallel computing with automatic processing of missing values, which significantly improves the computational efficiency of large-scale spatial datasets (Chen and Guestrin.,2016).

3. Results

https://doi.org/10.5194/egusphere-2025-2843
Preprint. Discussion started: 28 July 2025

3.1 Validation of the applicability of baseflow separation methods

We counted the best separation methods filtered in the Baseflow library for baseflow separation for each hydrological station data. From the results in Fig. 2, 28% of the hydrological stations are suitable for baseflow separation using the graphical method, 71% of the stations are suitable for baseflow separation using the digital filter method, and 1% of the stations have no obvious suitable separation method. Among them, the EWMA method is the most effective for baseflow separation in karst area, with 24% of hydrological stations suitable for baseflow separation, followed by the Eckhardt method, with 21% of hydrological stations suitable for baseflow separation.

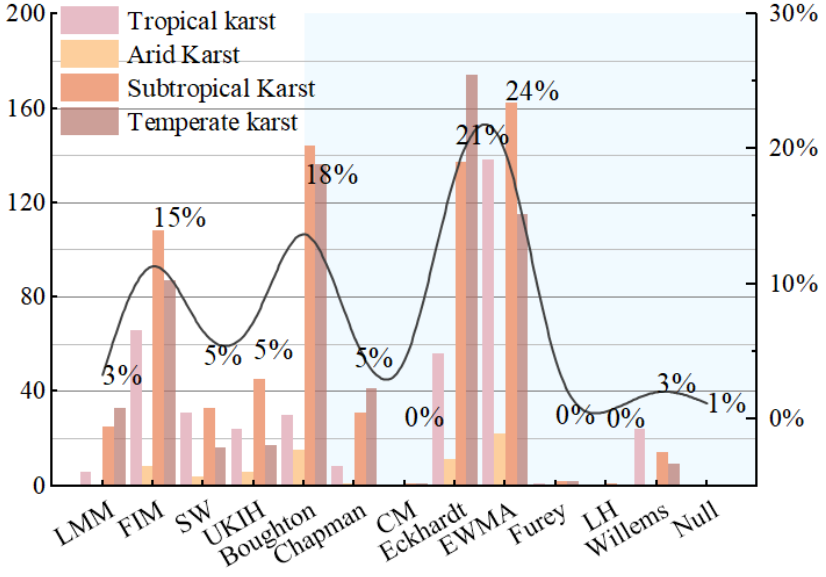

Figure 2. Percentage of best separation methods in the karst region and number of best separation methods in each climatic zone. Graphical methods are shown within the white background, digital filtering methods are shown within the light blue background, and different coloured bars correspond to different climatic zones.The X-axis shows the 12 baseflow separation methods, the Y-axis (left) shows the number of hydrological stations, and the Y-axis (right) shows the number of hydrological stations covered by each of the optimal baseflow separation methods as a proportion of the number of all hydrological stations, which corresponds to the black curve.

Figure 3(a) shows the KGE coefficient distributions of different methods, from the results, some digital filtering methods (orange) have concentrated KGE coefficient distributions and the values are close to 1. For example, the five methods, Boughton, Eckhardt, EWMA, Furey, and Willems, which indicate that the applicability of these

https://doi.org/10.5194/egusphere-2025-2843
Preprint. Discussion started: 28 July 2025

five base-flow separation methods is high and effective in the karst region. The KGE coefficients of the graphical method (green) are also well distributed, with most of the KGE coefficient distribution ranges greater than 0.5 and the average KGE coefficients of each method are greater than 0.75. It indicates that the graphical method also has high applicability in the karst region. On the other hand, the three digital filtering methods of Chapman, CM and LH have discrete distributions from the distribution of KGE coefficients, although their average values are all greater than 0.5. It indicates that the results obtained by these three methods are more fluctuating when dealing with data from different hydrological stations, and it also shows that these three methods are less stable when performing baseflow separation.

The distribution pattern of the NSE coefficients of the different methods in Fig. 3(b) is similar to that of Fig. 3(a). The NSE coefficients of the five methods, Boughton, Eckhardt, EWMA, Furey, and Willems, have a concentrated distribution and high mean values, which further suggests that these five methods are effective in separating the baseflow in karst regions. The distribution of NSE coefficients of the four graphical methods (in green) is generally stable although the range of NSE coefficients increases compared to the KGE coefficients, and their mean values are all greater than 0.5. The distribution of NSE coefficients of the three digital filtering methods of Chapman, CM, and LH is still more discrete (-0.5 to 1), which further indicates that the applicability of these methods in karstic regions is low.

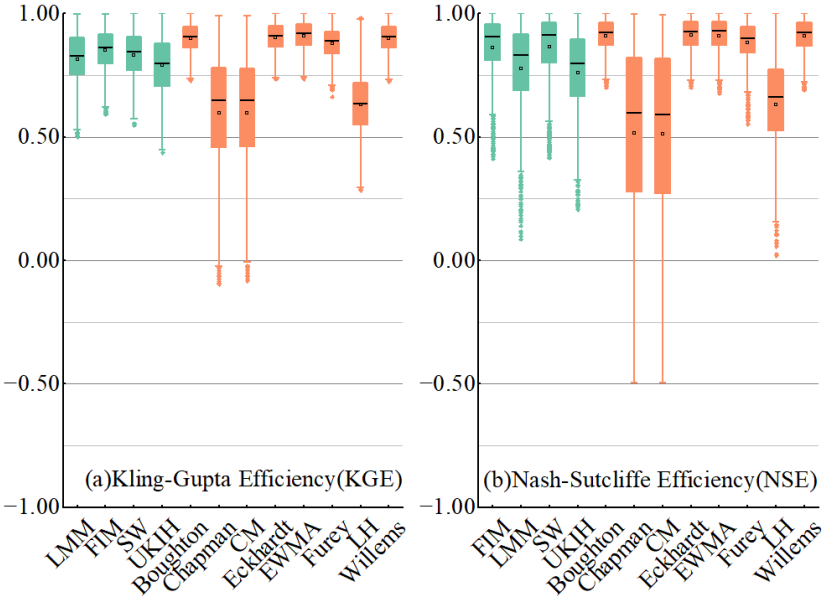

https://doi.org/10.5194/egusphere-2025-2843
Preprint. Discussion started: 28 July 2025

Figure 3. KGE coefficients (a) versus NSE coefficients (b) for 12 baseflow separation methods. The X-axis indicates each separation method and the Y-axis indicates the value of the coefficients. The green color in the graph indicates the graphical method and the orange color indicates the digital filtering method. The black lines within the boxplot indicate the mean values, with upper and lower limits of 1.5 times Interquartile Range(IQR), and exceeding the range is considered as an outlier, which is labeled in the form of dots at the top and bottom of the boxplot.

From the distribution characteristics of KGE and NSE coefficients in different climatic zones (Figure 4), the KGE coefficients of multiple separation methods in tropical karst have discrete distributions, with CM and Chapman ranging from -1.5 to 1. The NSE coefficients are similar to those of the KGE, but with a relatively centralised distribution. The distribution of coefficients of graphical methods in the arid karst region are all discrete, and the digital filtering method is still the CM and Chapman methods presenting a low concentration. The distribution of KGE coefficients in subtropical and temperate karst is relatively stable and concentrated, and the overall distribution of KGE coefficients of Chapman and CM are also discrete, while the KGE coefficients of FIM and SW are close to 1, which indicates that these methods are more effective in separating the baseflow in subtropical and temperate karst regions.

According to Figures 2 and 3, considering the high KGE and NSE coefficients and the number of most suitable hydrological stations, we selected four more suitable methods for baseflow separation in karst regions, which are one graphical method (FIM) and three digital filtering methods (Boughton, Eckhardt, EWMA).

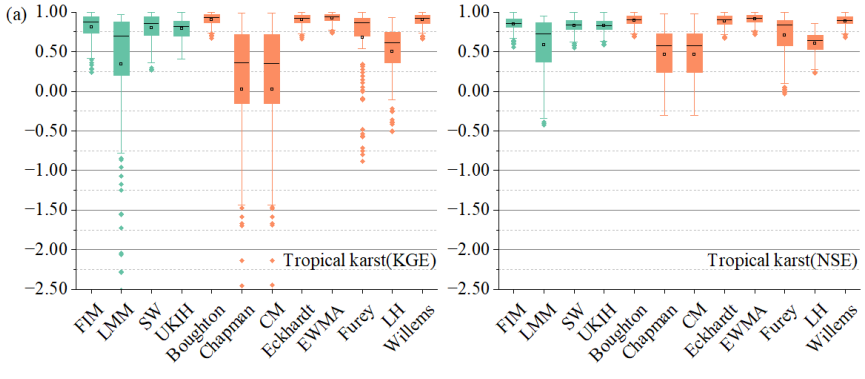

https://doi.org/10.5194/egusphere-2025-2843
Preprint. Discussion started: 28 July 2025

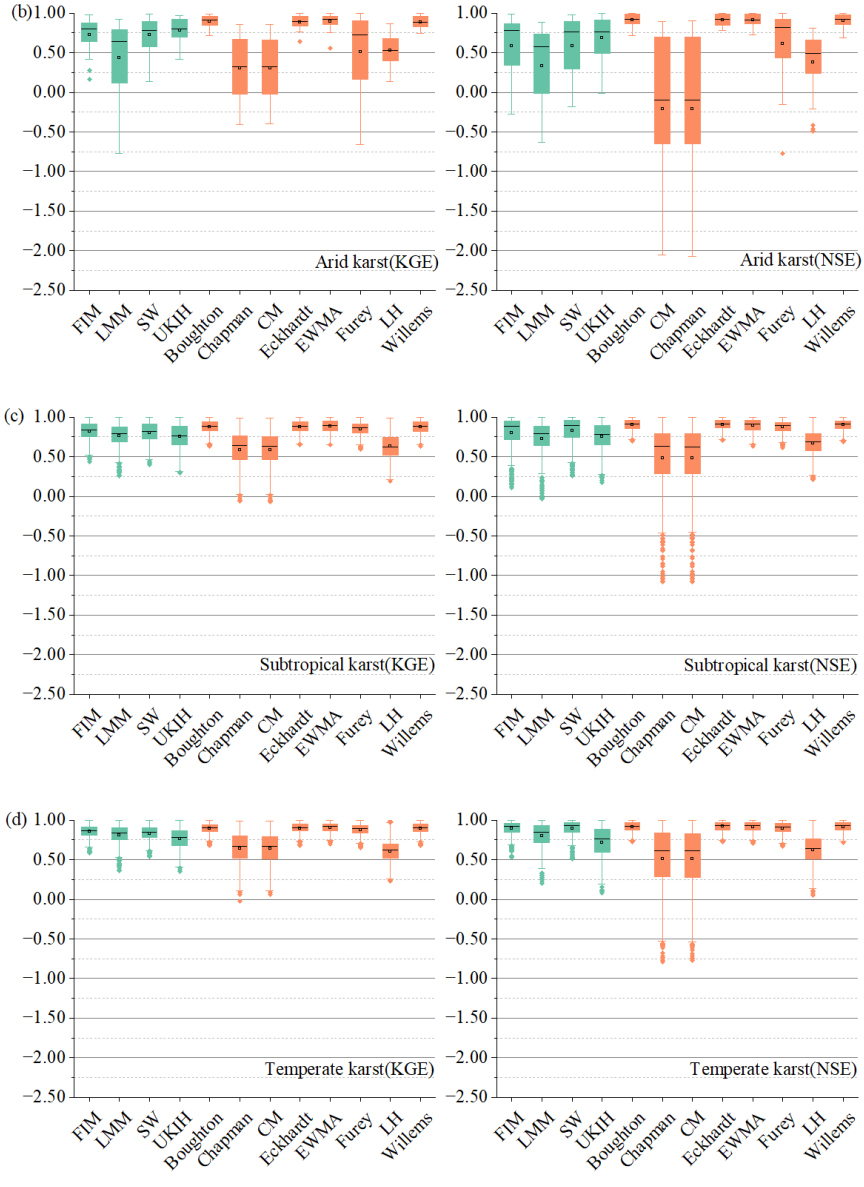

Figure 4. KGE coefficients (left column) versus NSE coefficients (right column) for karst regions in different climatic zones (labeled at the bottom right of each component Figures). The X-axis indicates each separation method and the Y-axis indicates the value of the coefficients. The green color in the graph indicates the graphical method and the orange color indicates the digital filtering method. The black lines within the boxplot indicate the mean values, with upper and lower limits of 1.5 times IQR, and

https://doi.org/10.5194/egusphere-2025-2843
Preprint. Discussion started: 28 July 2025

exceeding the range is considered as an outlier, which is labeled in the form of dots at the top and bottom of the boxplot.

3.2 Differences in baseflow indices obtained by different methods over time

From Figure 5a, it can be found that the four graphical methods have different effects on baseflow separation in karst regions. Among them, the BFIs derived by FIM and SW are similar, with an average value of about 86%. Moreover, the BFI shows an increasing trend of low amplitude with the year, with low fluctuation degree and high stability. The mean value of BFI derived from LMM is about 83%, and the trend of change with years shows a decreasing and then increasing trend, while the result of UKIH method is low, with a mean value of about 77%, and its BFI also shows a slow increasing trend with years.

The results in Figure 5b can be found that although there are differences in the base flow indices obtained by different digital filtering methods, most of the methods obtain similar base flow indices and have similar trends with respect to year. In contrast, the results of the two methods Chapman and CM differ significantly from those of the other six methods. The mean value of the BFI obtained by the two methods is about 58%, and there is a small decrease followed by a slow increase in the trend.

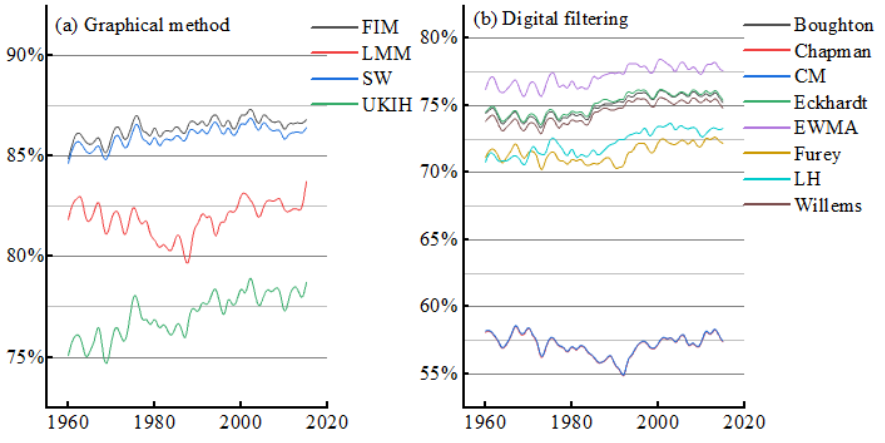

Figure 5. Global BFIs for karst regions calculated by the 12 baseflow separation methods, with the x-axis indicating the year and the y-axis the BFI.

In order to analyze the reasons for the differences between these two methods (CM and Chapman) and other methods in separating baseflows, we selected one hydrological station in each climatic zone and generated baseflow curves obtained by the different methods in different climatic zones (Figure 6). Since the CM method is an improvement

https://doi.org/10.5194/egusphere-2025-2843
Preprint. Discussion started: 28 July 2025

of Chapman by adding a maximum baseflow limit to the Chapman method, and its internal mechanism is consistent, Chapman was used as a proxy. In addition, the Eckhardt method with high KGE and NSE coefficients is chosen as a comparison. From Figure 6, we find that when runoff increases, the Eckhardt method can respond quickly and baseflow increases rapidly, while the Chapman method responds to the increase in runoff to a lesser extent and by a lower amount than Eckhardt. Overall, Chapman responds more slowly to the recharge of precipitation than the other methods, and this feature also makes the Chapman method less discriminating for baseflow compared to the other methods.

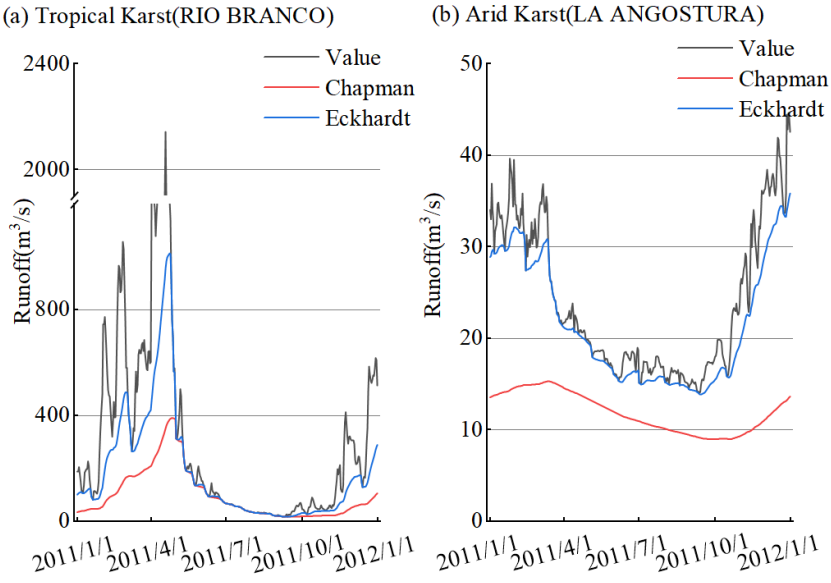

https://doi.org/10.5194/egusphere-2025-2843
Preprint. Discussion started: 28 July 2025

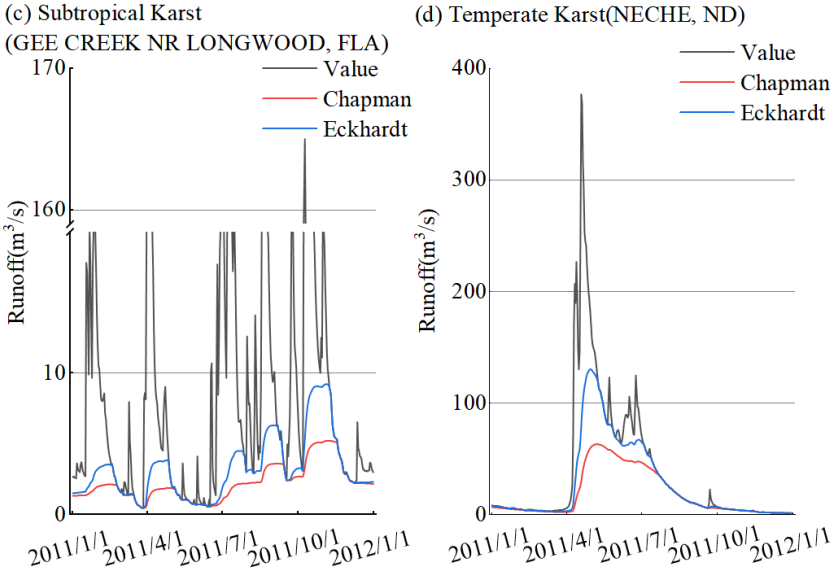

Figure 6. baseflow curves for different climatic zones (Eckhardt and Chapman methods were chosen as representatives), where the X-axis represents time and the Y-axis represents runoff. The black curve (Value) represents the runoff volume. Names of hydrological stations are in parentheses.

3.3 Global base flow characteristics

In order to more clearly characterize the BFI in karst basins, we calculated the BFI in non-karst basins globally using the same method. Figure 7 shows that BFIs in karst basins are significantly higher than in non-karst basins. The BFI of karst basins is 78±6.9%, while the BFI of non-karst basins is about 60%. This indicates that baseflow in karst basins is significantly underestimated if only global average conditions are considered and baseflow in karst basins is not calculated separately.

As can be seen from Figure 7, there are differences in the characteristics of BFIs over time in different climatic zones. The BFI in the tropical karst region generally shows an increasing trend. From 1960 to about 1990, the base flow index in tropical karst showed an increasing trend, and since 1990 the base flow index remained at about 80% and then stabilized. The BFI in arid karst region is the highest, with a mean value of about 85%. In general, the BFI in arid karst region shows a decreasing trend, and the annual mean BFI fluctuates greatly, with poor stability. The BFI of subtropical karst region is more stable, always maintained at about 78%. The characteristics of BFI in temperate karst regions are similar to those of tropical karst, showing a slow increase and remaining stable at around 80%.

https://doi.org/10.5194/egusphere-2025-2843
Preprint. Discussion started: 28 July 2025

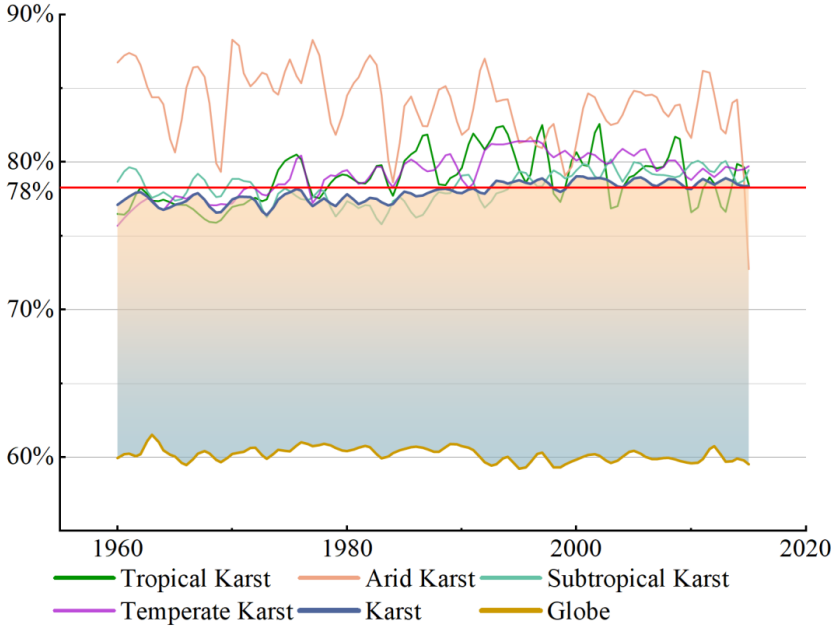

Figure 7. Annual BFIs for each region of global karst versus global annual BFIs. x-axis indicates the year, y-axis indicates the BFI, and the red straight line is the overall mean of the BFI. The orange curve at the bottom indicates the global BFI, and the dark blue line indicates the BFI for global karst regions.

The average of BFIs obtained by the four methods (FIM, Boughton, Eckhardt, EWMA) was used as the BFI for the global karst region and linearly regressed against the year (Figure 8). The results show an increasing trend in the BFI in the global karst region, with an increase of about 1.5% from 1960 to 2015. One of the obvious increase periods is from 1980 to 2000. Since 2000, the BFI in the global karst region has stabilised, fluctuating in the range of 78.5% ± 0.5%.

https://doi.org/10.5194/egusphere-2025-2843
Preprint. Discussion started: 28 July 2025

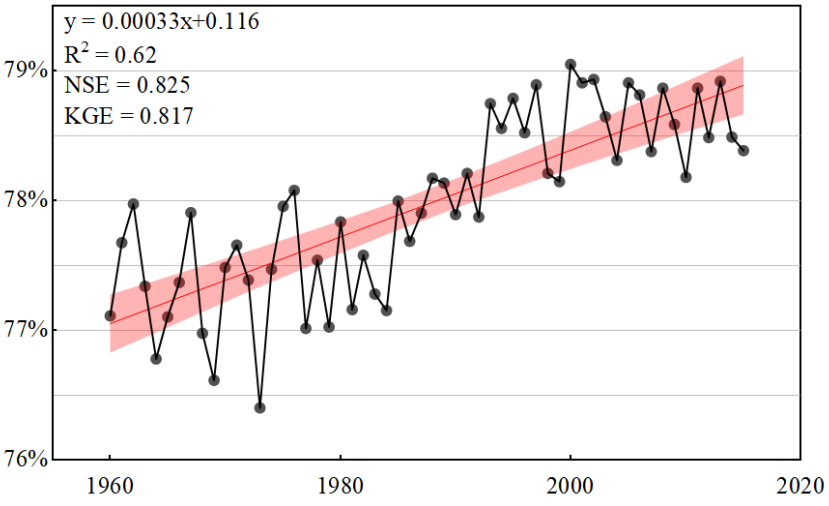

Figure 8. Annual mean BFIs over time for global karst regions. x-axis indicates year, y-axis indicates BFIs, and red bars indicate 95% confidence interval.

Figure 9 shows that, despite being in the same climatic zone, different regions can exhibit differences in BFIs. For example, in the northern part of South America and the Southeast Asian region, which are both tropical karst, the BFI is significantly higher in the Southeast Asian region (81%) than in the northern part of South America (73%). There is also a significant difference in BFIs between the eastern part of the United States and the northern part of Africa, which are both arid karst climate zones. From figure 9 and figure 10 we find that BFI stability is lower and BFI values are higher in arid karst regions. The degree of variation of BFI in tropical karst regions is lower than that in arid karst regions. And subtropical and temperate karst regions have the lowest trend of base flow index change and their stability is higher.

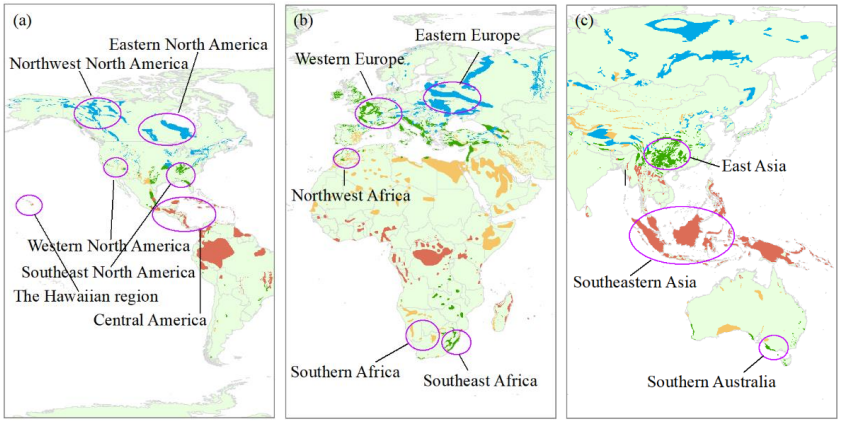

https://doi.org/10.5194/egusphere-2025-2843
Preprint. Discussion started: 28 July 2025

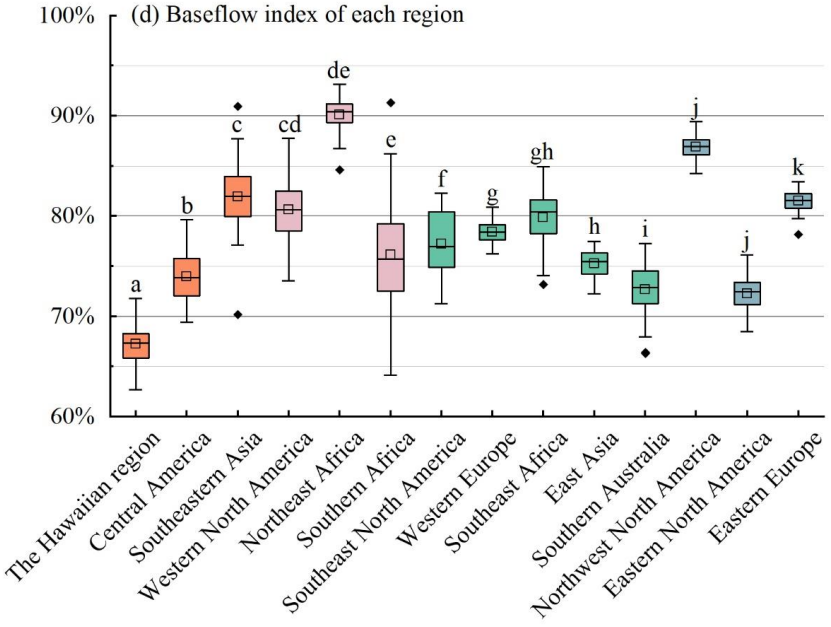

Figure 9. Distribution of BFIs in karst basins in different regions within the same climatic zone. In figure (d), orange represents tropical karst regions, magenta represents arid karst regions, green bars represent subtropical karst regions, and brownish-purple represents temperate karst regions.

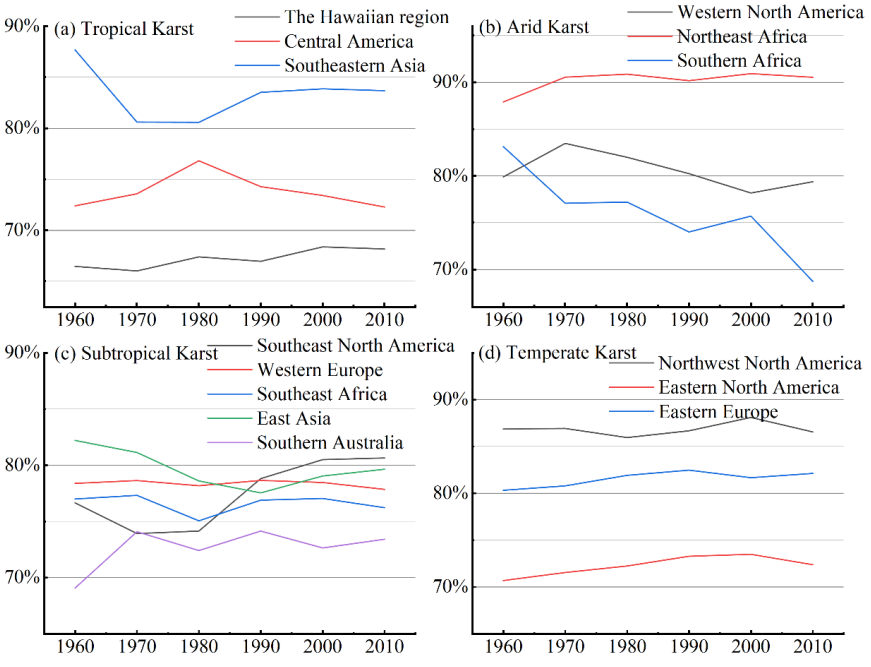

https://doi.org/10.5194/egusphere-2025-2843
Preprint. Discussion started: 28 July 2025

Figure 10. Characteristics of BFIs with respect to year for different regions within the same climatic zone. Where Y-axis indicates BFI and X-axis indicates year.

3.4 Factors influencing baseflow indices in karst regions

Using the XGBoost model, we conducted an attribution analysis of the 12 factors that may affect the BFI (Figure 11), and finally concluded that Gross Primary Productivity (GPP) has the greatest influence on baseflow, reaching 15.0%. Elevation was the next most influential factor with 12.4%, in addition to this, slope and runoff volume (Flow) also had a large influence (>10%) on base flow index. In contrast, climatic factors such as relative humidity (RH), Land-surface radiation (SR) and air temperature (Temp) had a low influence on base flow index, each characterized by less than 5%.

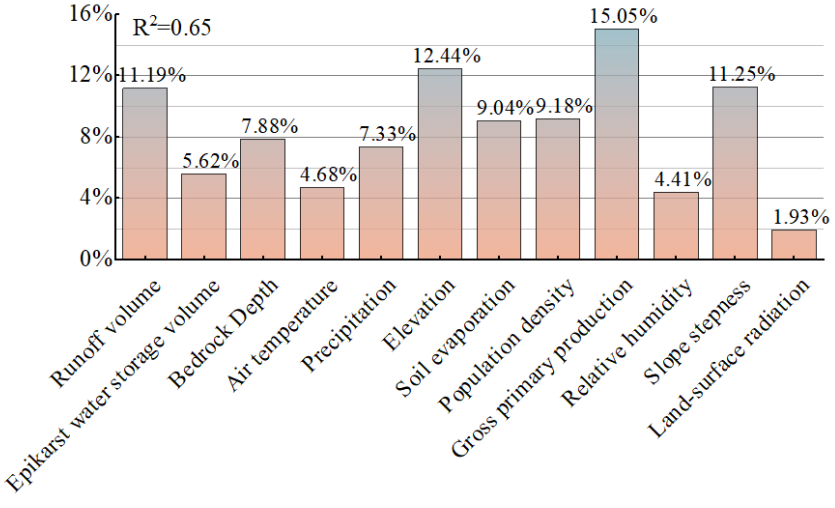

Figure 11. Influence of different factors on baseflow, where the X-axis indicates different factors, the Y-axis indicates the contribution of the influencing factor to the baseflow, and the number above the bar indicates the contribution of the current factor.

4. Discussion

4.1 Mechanisms of formation of baseflow characteristics in karst regions

The results of the study show that the BFI in karst regions is significantly higher than the global average (Figure 7). We attribute this difference to the unique geological structure and hydrological cycle characteristics of karst regions. Extensively developed fissures, vertical seepage zones, and subsurface dissolution piping systems in karst

https://doi.org/10.5194/egusphere-2025-2843
Preprint. Discussion started: 28 July 2025

regions constitute complex hydrological channels, which significantly alter surface water-groundwater exchange patterns (Ford & Williams, 2007; Li et al., 2024). Compared with the homogeneous water storage medium dominated by fissures and pores in non-karst areas, the network of dissolution channels in karst regions significantly shortens the infiltration path of precipitation, and its infiltration rate can reach several to tens of times of that in non-karst areas(Fu et al .,2016). For example, the monitoring of karst slopes in Huanjiang, Guangxi, shows that the wet front transport rate is as high as 1373 mm/h, compared with 17-610 mm/h in non-karst regions, which indicates that the rate of water infiltration in karst regions is much higher than that in non-karst regions (Medici et al., 2019; Zhang et al., 2024). This part of precipitation recharge into the subsurface, under the action of gravity and pressure, squeezes the 'old water' out of the underground aquifer, which indirectly enhances the baseflow ratio (Reimann et al., 2011; Bailly-Comte et al., 2010; Evans. 1983; Ronayne. 2013). Studies have shown that this mechanism can result in significantly higher baseflow contributions in karst regions, even above 80% in specific environments (Zhang et al., 2022), whereas only less than 50% of precipitation can be converted to baseflow in non-karst regions due to the blocking effect of loose sedimentary layers (Cusano et al., 2024).

Significant differences in surface cover conditions further reinforce baseflow differences. In some karst areas, bedrock is exposed to more than 60%, and thin layers of residual soil (<30 cm) cover only 20% of the surface, a geologic feature that results in reduced surface interception and elevated subsurface recharge (Anker et al., 2023;Li et al .,2024 ;Wang et al .,2024). The karst fissure system is directly exposed to the atmospheric interface, avoiding water loss through evaporation from the soil layer, and the lack of continuous surface cover allows for direct infiltration of large amounts of precipitation (Yang et al., 2025; Li et al., 2023). On the contrary, in non-karst areas, the soil-vegetation system formed by thicker weathered crust constitutes a natural evapotranspiration interface, and the average annual evapotranspiration can reach 40% of the precipitation, and surface runoff accounts for 30% of the precipitation, which significantly weakened the intensity of groundwater recharge (Jiang et al., 2020; Wang et al., 2020; Wetzel et al.,1996). This double hydrological barrier effect ultimately leads to systematic differences between BFIs in karst regions and non-karst regions.

4.2 Reasons for differences in baseflow in karst regions in different climatic zones

https://doi.org/10.5194/egusphere-2025-2843
Preprint. Discussion started: 28 July 2025

The results show that BFIs in karst regions in different climatic zones exhibit significant differences (Figure 9 and Figure 10). The underlying driving force lies in the heterogeneity of the geologic structure and its coupling effect with long-term climatic erosion(Liu et al .,2023). Among them, the control of the spatial structure of the water storage medium by the geologic context is the decisive factor for the differences in BFIs(Luo et al ., 2023). For example, in Southeast Asian karst regions (e.g., Halong Bay, Vietnam), the development of high-purity, thick-bedded limestone, and the formation of a pipeline network with vertical dominance under the background of tectonic uplift, the short groundwater runoff paths and efficient recharge mechanisms directly enhance the baseflow (Duringer et al., 2012). In contrast, siliceous interbedding in dolomite formations in northern South America (e.g., Caatinga, Brazil) significantly increases the resistance to dissolution and reduces the connectivity of the dissolution network, a primary geologic feature that fundamentally constrains the baseflow (Teixeira et al., 2023). The intensity of tectonic activity and the stage of geomorphic evolution further strengthen regional differences. For example, strong Cenozoic uplift in Southeast Asia formed steep young landforms that promoted vertical permeability dominance. In contrast, Paleozoic stable landmasses in northern Africa (e.g., the Saharan Atlas Mountains) are dominated by horizontal cave systems, a geologic feature that also makes the baseflow in this region significantly different from other regions (Klimchouk, 2007; Jiang et al., 2020). Surface cover characteristics are equally critical as secondary geologic elements. For example, thicker soil layers in temperate zones (e.g., Slovenia) increase surface runoff diversion through delayed infiltration, whereas large areas of exposed bedrock in equatorial zones infiltrate directly through solution gaps, creating a multiplicative effect on the BFI (Li et al., 2023).

Climate elements reshape geological structures over large time scales through geological erosion processes, thereby indirectly influencing baseflow patterns. While short-term hydrological dynamics are affected by climate parameters such as precipitation intensity and seasonal distribution (Mo et al., 2021 ; Cheng et al .,2023), the profound control of climate on the baseflow index is evident in its long-term modification of karst systems. For example, the strong coupling of heavy precipitation and high temperatures in equatorial regions significantly accelerates the dissolution of carbonate rocks, forming a dense network of highly permeable dissolution fissures. Conversely, the persistent moisture associated with temperate maritime climates enhances the dissolution of carbonate rocks (with an average annual dissolution rate

https://doi.org/10.5194/egusphere-2025-2843
Preprint. Discussion started: 28 July 2025

approximately 40% higher than that of non-karst areas at the same latitude), leading to the formation of cave clusters characterized by labyrinthine structures and interwoven underground river systems. This climate-driven differentiation in dissolution alters the capacity of groundwater storage spaces, ultimately reflecting in the characteristic values of regional baseflow indices (Ford and Williams, 2007; Goldscheider, 2015; Tapiador et al., 2012).

4.3 Reasons for changes in baseflow indices over time

The results of the experiment revealed an increasing trend in the BFI in the karst region (Figure 8). Although the degree of increase is low (about 1.5% from 1960 to 2015), we still feel that this degree of increase in BFI is a cause for concern given that the average BFI in the karst region is already at a high level. The reason for the increasing trend in BFI in the karst region is presumably caused by the large loss of groundwater. Extensive monitoring has shown that groundwater levels globally show a rapid declining trend, and this systematic attenuation has triggered multiple crises such as basin hydrological process anomalies and regional climate feedback imbalances (Jasechko et al., 2024, de Graaf et al. 2019; Liu et al.,2015). It is the rapid decline of the water table that leads to a constant unsaturated state of groundwater storage. Therefore, when recharged by precipitation, large amounts of precipitation preferentially fill the void in the water table, making the generation of surface runoff require longer recharge cycles.

In addition to this, the geological and hydrological characteristics of the karst region further amplify this effect of reduced surface runoff and increased Baseflow (Zhu et al.,2025). On the one hand, there is the rapid water-conducting effect of the karst fissure network, where the extensive development of dissolution pipes and fissures in the karst bedrock accelerates vertical infiltration of precipitation into deep groundwater, leading to difficulties in retaining soil moisture and a significant increase in the runoff generation threshold (Hartmann et al., 2014). On the other hand, there is the dissipative effect of the surface-subsurface dichotomy, where the thickness of the unsaturated zone of the karst aquifer increases in the context of persistent groundwater overdraft (D'Ettorre et al., 2024), further weakening the immediate contribution of precipitation events to runoff.

4.4 Applicability and limitations of this study

With regard to data sources, the original data sources are diverse and complex.

https://doi.org/10.5194/egusphere-2025-2843
Preprint. Discussion started: 28 July 2025

Although we have made a lot of efforts to eliminate a large number of original documents with distorted data and to screen out some unreasonable data in the calculation, it is always difficult to fully balance the deficiencies in the original data.

On the boundaries of applicability of the method itself. For example, the parameterization framework of digital filtering methods (e.g., Eckhardt and Chapman algorithms) based on the assumption of linear recession is at variance with the nonlinear characteristics of karst hydrological processes. Together with the rapid recession processes dominated by karst pipe flow (rates up to 2-3 times that of porous media basins) leads to a general underestimation of the recession coefficient (Kang et al 2022; Rattayová & Hlavčová., 2023), which leads to differences in baseflow separation between methods with different principles. For example, the Chapman and CM methods used in this study, from the results of the two methods, the separation of baseflow is significantly lower than the other methods, which is due to the lower degree of response of the Chapman and CM methods to precipitation recharge, which is also reflected in Helfer's study (Helfer et al., 2024). In addition, empirical parameters such as maximum baseflow (BFI_max) are mostly derived from rate-determined results for temperate homogeneous aquifers, and their physical mechanisms have not been fully adapted for applicability in karst regions (Zhou et al., 2017).

Despite the above limitations, this study ensures the spatial representativeness and methodological reliability of the study conclusions by integrating a global-scale multi-source dataset of karst region (covering more than 85% of the typical karst geomorphological units) and adopting standardized validation indexes (KGE, NSE). The results show that the karst baseflow separation results can effectively characterize the regional hydrological features and provide data support for water resource management and eco-hydrological model construction in karst region. Future research can integrate geophysical exploration and isotope tracer technology to develop a dynamic parameterization scheme adapted to non-homogeneous media.

5. Conclusion

This study systematically analyzes the spatial distribution characteristics and trends of BFIs in global karst regions. The results show that the BFI (78%) in karst regions is generally significantly higher than the global BFI. This phenomenon confirms the differential regulation of the runoff partitioning mechanism by the unique surface-groundwater dichotomy in karst regions. Meanwhile, the study systematically evaluates the applicable boundary of the hydrographic method in karst region and proves the

https://doi.org/10.5194/egusphere-2025-2843
Preprint. Discussion started: 28 July 2025

applicability of the hydrographic method in karst region. It is noteworthy that the BFI in the karst region shows a phased upward trend against the background of the general decay of global groundwater reserves. This may be related to the buffering effect of karst aquifers on extreme climatic events and human activity-induced changes in the subsurface bedding. In future research, we can integrate high-precision geological tectonic data and multi-source remote sensing information to construct a coupled climate-hydrology-geology model to quantitatively analyze the response characteristics of hydrological fluxes of karst systems under the background of climate change, and further improve the spatial and temporal resolution dimensions of karst water cycle theory.

https://doi.org/10.5194/egusphere-2025-2843
Preprint. Discussion started: 28 July 2025

Declaration of the Competing Interest

The authors declare that they have no known competing financial interests o r personal relationships that could have appeared to influence the work reported in this paper

Acknowledgments

This study was supported by the National Natural Science Foundation of China (42461004, U1812401, U1612441); Science and Technology Plan Project of Guizhou Province (Qiankehejichu-ZK[2025] Zhongdian 045; Qiankehejichu-ZK[2025] Mianshang 268)

References:

Mukherjee, A., Bhanja, S.N. & Wada, Y. Groundwater depletion causing reduction of baseflow triggering Ganges river summer drying. *Sci Rep* **8**, 12049 (2018). https://doi.org/10.1038/s41598-018-30246-7

Chen, H., Chen, Y., Li, W., & Li, Z. (2019). Quantifying the contributions of snow/glacier meltwater to river runoff in the Tianshan Mountains, Central Asia. *Global and Planetary Change*, *174*, 47-57. https://doi.org/10.1016/j.gloplacha.2019.01.002

Saedi, J., Sharifi, M.R., Saremi, A. *et al.* Assessing the impact of climate change and human activity on streamflow in a semiarid basin using precipitation and baseflow analysis. *Sci Rep* **12**, 9228 (2022). https://doi.org/10.1038/s41598-022-13143-y

Hare, D.K., Helton, A.M., Johnson, Z.C. *et al.* Continental-scale analysis of shallow and deep groundwater contributions to streams. *Nat Commun* **12**, 1450 (2021). https://doi.org/10.1038/s41467-021-21651-0

Yang, C., Condon, L.E. & Maxwell, R.M. Unravelling groundwater–stream connections over the continental United States. *Nat Water* **3**, 70–79 (2025). https://doi.org/10.1038/s44221-024-00366-8

Zhang, J., Song, J., Cheng, L., Zheng, H., Wang, Y., Huai, B., Sun, W., Qi, S., Zhao, P., Wang, Y., & Li, Q. (2019). Baseflow estimation for catchments in the Loess Plateau, China. Journal of Environmental Management, 233, 264-270. https://doi.org/10.1016/j.jenvman.2018.12.040

Mei, Y., Wang, D., Zhu, J., Tang, G., Cai, C., Shen, X., et al. (2024). Optimal baseflow separation through chemical mass balance: Comparing the usages of two tracers, two concentration estimation methods, and four baseflow filters. *Water Resources Research*, 60, e2023WR036386. https://doi.org/10.1029/2023WR036386

Kuehne, L. M., Dickens, C., Tickner, D., Messager, M. L., Olden, J. D., O'Brien, G., Lehner, B., & Eriyagama, N. (2023). The future of global river health monitoring. *PLOS Water*, *2*(9), 1-27. Article e0000101. https://doi.org/10.1371/journal.pwat.0000101

Xie, J., Liu, X., Jasechko, S. *et al.* Majority of global river flow sustained by groundwater. *Nat. Geosci.* **17**, 770–777 (2024). https://doi.org/10.1038/s41561-024-01483-5

Beck, H. E., A. I. J. M. van Dijk, D. G. Miralles, R. A. M. de Jeu, L. A. Bruijnzeel, T. R. McVicar, and J. Schellekens (2013), Global patterns in base flow index and recession based on streamflow observations from 3394 catchments, *Water Resour. Res.*, 49, 7843–7863, doi:10.1002/2013WR013918.

https://doi.org/10.5194/egusphere-2025-2843
Preprint. Discussion started: 28 July 2025

583 Lyu, S., Guo, C., Zhai, Y., Huang, M., Zhang, G., Zhang, Y., Cheng, L., Liu, Q., Zhou, Y., Woods,
584 R., Zhang, J., & 11 others. (2023). Characterising baseflow signature variability in the Yellow River
585 Basin. Journal of Environmental Management, 345, 118565.
586 https://doi.org/10.1016/j.jenvman.2023.118565
587 Zhang, J., Song, J., Cheng, L., Zheng, H., Wang, Y., Huai, B., ... & Li, Q. (2019). Baseflow
588 estimation for catchments in the Loess Plateau, China. *Journal of environmental management*, *233*,
589 264-270.
590 Zhang, J., Song, J., Cheng, L., Zheng, H., Wang, Y., Huai, B., … & Li, Q. (2019). Baseflow
591 estimation for catchments in the Loess Plateau, China. Journal of Environmental Management, 233,
592 264-270. https://doi.org/10.1016/j.jenvman.2018.12.040
593 Jing, J., Li, R., Xiao, L., Shu, D., & Yang, P. (2024). Interpreting and modelling the daily extreme
594 sediment events in karst mountain watersheds. Science of The Total Environment, 926, 171956.
595 https://doi.org/10.1016/j.scitotenv.2024.171956
596 Ford, D., & Williams, P. (2007). karst Hydrogeology and Geomorphology. John Wiley & Sons Ltd.
597 https://doi.org/10.1002/9781118684986
598 Rosmalinda Permatasari, Arwin Sabar, Dantje Kardana Natakusumah, & Hazairin Samaulah. (2019).
599 EFFECTS OF WATERSHED TOPOGRAPHY AND LAND USE ON BASEFLOW
600 HYDROLOGY IN UPSTREAM KOMERING SOUTH SUMATERA, INDONESIA. GEOMATE
601 Journal, 17(59), 28–33. Retrieved from https://geomatejournal.com/geomate/article/view/251
602 Khomsiati, N. L., Suryoputro, N., Yulistyorini, A., Idfi, G., & Alias, N. E. B. (2021). The effect of
603 forest area change in tropical islands towards baseflow and streamflow. IOP Conference Series:
604 Earth and Environmental Science, 847, 012032. https://doi.org/10.1088/1755-1315/847/1/012032
605 Longobardi A, Van Loon AF. Assessing baseflow index vulnerability to variation in dry spell length
606 for a range of catchment and climate properties. *Hydrological Processes*. 2018; 32: 2496–
607 2509. https://doi.org/10.1002/hyp.13147
608 Guisiano, P. A., Santoni, S., Huneau, F., Mattei, A., & Garel, E. (2024). Using natural tracers and
609 calibrated analytical filter to highlight baseflow contribution to mountainous Mediterranean rivers
610 in a context of climate change. Journal of Hydrology, 641, 131842.
611 https://doi.org/10.1016/j.jhydrol.2024.131842
612 Mo, C., Ruan, Y., Xiao, X., Lan, H., & Jin, J. (2021). Impact of climate change and human activities
613 on the baseflow in a typical karst basin, Southwest China. Ecological Indicators, 126, 107628.
614 https://doi.org/10.1016/j.ecolind.2021.107628
615 Luo, Y., Zhou, Q., Peng, D., Yan, W., & Zhao, M. (2023). Key influence of hydrogeological,
616 geochemical, and geological structure factors on runoff characteristics in karst catchments. Journal
617 of Hydrology, 623, 129852. https://doi.org/10.1016/j.jhydrol.2023.129852
618 Li, Y., Zhou, Q. & Zhao, Y. Hydrologic response in a typical karst desertification catchment.
619 Carbonates Evaporites 39, 16 (2024). https://doi.org/10.1007/s13146-024-00929-6
620 Li, Y., Li, K., Zhou, Q., Zhao, Y., Cai, L., & Yang, Z. (2024). Spatiotemporal dynamics and similarity
621 in soil moisture in shallow soils on karst slopes. Journal of Hydrology, 639, 131655.
622 https://doi.org/10.1016/j.jhydrol.2024.131655
623 Zhu De-gen, Ning Jing, Yang Hui, Pu Jun-bing, Cao Jian-hua, Zhou Meng-xia, Prelovšek Mitja,
624 Ravbar Nataša. 2025. Research hotspot and trend of plant water use in karst: Based on a bibliometric
625 analysis from 1984 to 2022. China Geology, 8(1), 214–229. doi: 10.31035/cg2023134.
626 Cheng, S., Yu, X., Li, Z., Xu, X., Gao, H., & Ye, Z. (2023). The effect of climate and vegetation

https://doi.org/10.5194/egusphere-2025-2843
Preprint. Discussion started: 28 July 2025

variation on monthly sediment load in a karst watershed. *Journal of Cleaner Production, 382*, 135290. https://doi.org/10.1016/j.jclepro.2022.135290

Tobin BW, Schwartz BF. Quantifying the role of karstic groundwater in a snowmelt-dominated hydrologic system. *Hydrological Processes*. 2020; 34: 3439–3447. https://doi.org/10.1002/hyp.13833

Tobin BW, Schwartz BF. Quantifying the role of karstic groundwater in a snowmelt-dominated hydrologic system. *Hydrological Processes*. 2020; 34: 3439–3447. https://doi.org/10.1002/hyp.13833

Mo, C., Jiang, C., Long, S., & Cen, W. (2025). Comprehensive evaluation and attribution analysis of baseflow variation in a typical karst basin, Southwest China. Journal of Hydrology: Regional Studies, 57, 102185. https://doi.org/10.1016/j.ejrh.2025.102185

Foran Quinn, D., Murphy, C., Wilby, R. L., Matthews, T., Broderick, C., Golian, S., … Harrigan, S. (2021). Benchmarking seasonal forecasting skill using river flow persistence in Irish catchments. *Hydrological Sciences Journal*, *66*(4), 672–688. https://doi.org/10.1080/02626667.2021.1874612

Lyu, S., Zhai, Y., Zhang, Y., Cheng, L., Paul, P. K., Song, J., Wang, Y., Huang, M., Fang, H., & Zhang, J. (2022). Baseflow signature behaviour of mountainous catchments around the North China Plain. Journal of Hydrology, 606, 127450. https://doi.org/10.1016/j.jhydrol.2022.127450

Tagne, G. V. and Dowling, C., "Inferring groundwater flow and recharge from time series analysis of storm responses in a karst aquifer of southeastern Kentucky (USA)" (2018). KIP Articles. 2659.https://digitalcommons.usf.edu/kip_articles/2659

Guisiano, P. A., Santoni, S., Huneau, F., Mattei, A., & Garel, E. (2024). Using natural tracers and calibrated analytical filter to highlight baseflow contribution to mountainous Mediterranean rivers in a context of climate change. Journal of Hydrology, 641, 131842. https://doi.org/10.1016/j.jhydrol.2024.131842

He, Z., Unger-Shayesteh, K., Vorogushyn, S., Weise, S. M., Kalashnikova, O., Gafurov, A., Duethmann, D., Barandun, M., & Merz, B. (2019). Constraining hydrological model parameters using water isotopic compositions in a glacierized basin, Central Asia. Journal of Hydrology, 571, 332-348. https://doi.org/10.1016/j.jhydrol.2019.01.048

Yang, Y., Weng, B., Yan, D., Gong, X., Dai, Y., Niu, Y., & Dong, G. (2021). Tracing potential water sources of the Nagqu River using stable isotopes. Journal of Hydrology: Regional Studies, 34, 100807. https://doi.org/10.1016/j.ejrh.2021.100807

Arnold, Jeffrey G. et al. “SWAT: Model Use, Calibration, and Validation.” *Transactions of the ASABE* 55 (2012): 1491-1508.

Wu, L., Wang, S., Bai, X., Luo, W., Tian, Y., Zeng, C., Luo, G., & He, S. (2017). Quantitative assessment of the impacts of climate change and human activities on runoff change in a typical karst watershed, SW China. Science of The Total Environment, 601–602, 1449-1465. https://doi.org/10.1016/j.scitotenv.2017.05.288

Lehner, B., Grill G. (2013). Global river hydrography and network routing: baseline data and new approaches to study the world’s large river systems. Hydrological Processes, 27(15): 2171–2186. https://doi.org/10.1002/hyp.9740

Li, Bailing, Rodell, Matthew, Sheffield, Justin, Wood, Eric, Sutanudjaja, Edwin. 2019. Long-term, non-anthropogenic groundwater storage changes simulated by three global-scale hydrological

https://doi.org/10.5194/egusphere-2025-2843
Preprint. Discussion started: 28 July 2025

671 models. *Scientific Reports*. Vol. 9, No. 1, pp. 10746. DOI: 10.1038/s41598-019-47219-
672 z ISSN: 2045-2322
673 Hengl, T., Mendes de Jesus, J., Heuvelink, G. B., Ruiperez Gonzalez, M., Kilibarda, M., Blagotić,
674 A., Shangguan, W., Wright, M. N., Geng, X., Bauer-Marschallinger, B., Guevara, M. A., Vargas, R.,
675 MacMillan, R. A., Batjes, N. H., Leenaars, J. G., Ribeiro, E., Wheeler, I., Mantel, S., & Kempen, B.
676 (2017). SoilGrids250m: Global gridded soil information based on machine learning. *PloS one*, *12*(2),
677 e0169748. https://doi.org/10.1371/journal.pone.0169748
678 arris, I., Osborn, T.J., Jones, P. *et al.* Version 4 of the CRU TS monthly high-resolution gridded
679 multivariate climate dataset. *Sci Data* **7**, 109 (2020).
680 Fick, S.E. and R.J. Hijmans, 2017. WorldClim 2: new 1km spatial resolution climate surfaces for
681 global land areas. International Journal of Climatology 37 (12): 4302-4315.
682 Wieder, W.R., J. Boehnert, G.B. Bonan, and M. Langseth. 2014. Regridded Harmonized World Soil
683 Database v1.2. ORNL DAAC, Oak Ridge, Tennessee, USA.
684 https://doi.org/10.3334/ORNLDAAC/1247
685 Bright, E., Rose, A., & Urban, M. (2013). *LandScan Global 2012* [Data set]. Oak Ridge National
686 Laboratory. https://doi.org/10.48690/1524215
687 Wild, B., Teubner, I., Moesinger, L., Zotta, R.-M., Forkel, M., van der Schalie, R., Sitch, S., and
688 Dorigo, W.: VODCA2GPP – a new, global, long-term (1988–2020) gross primary production dataset
689 from microwave remote sensing, Earth Syst. Sci. Data, 14, 1063–1085, https://doi.org/10.5194/essd-
690 14-1063-2022, 2022.
691 Tang, W. (2019). Dataset of high-resolution (3 hour, 10 km) global surface solar radiation (1983-
692 2018). National Tibetan Plateau / Third Pole Environment Data
693 Center. https://doi.org/10.11888/Meteoro.tpdc.270112.
694 Brutsaert, W. (2008), Long-term groundwater storage trends estimated from streamflow records:
695 Climatic perspective, *Water Resour. Res.*, 44, W02409, doi:10.1029/2007WR006518.
696 Rammal, M., Archambeau, P., Erpicum, S., Orban, P., Brouyère, S., Pirotton, M.,
697 & Dewals, B. (2018). Technical note: An operational implementation of recursive digital filter for
698 base flow separation. *Water Resources Research*, 54, 8528–
699 8540. https://doi.org/10.1029/2018WR023351
700 Xie, J., Liu, X., Wang, K., Yang, T., Liang, K., & Liu, C. (2020). Evaluation of typical methods for
701 baseflow separation in the contiguous United States. Journal of Hydrology, 583, 124628.
702 https://doi.org/10.1016/j.jhydrol.2020.124628
703 Nash, J. E., & Sutcliffe, J. V. (1970). River flow forecasting through conceptual models part I — A
704 discussion of principles. Journal of Hydrology, 10(3), 282-290. https://doi.org/10.1016/0022-
705 1694(70)90255-6
706 Gupta, H. V., Kling, H., Yilmaz, K. K., & Martinez, G. F. (2009). Decomposition of the mean
707 squared error and NSE performance criteria: Implications for improving hydrological modelling.
708 Journal of Hydrology, 377(1–2), 80-91. https://doi.org/10.1016/j.jhydrol.2009.08.003
709 Niazkar, M., Menapace, A., Brentan, B., Piraei, R., Jimenez, D., Dhawan, P., & Righetti, M. (2024).
710 Applications of XGBoost in water resources engineering: A systematic literature review (Dec 2018–
711 May 2023). *Environmental Modelling & Software*, *174*, 105971.
712 Zhang, J., Ma, X., Zhang, J., Sun, D., Zhou, X., Mi, C., & Wen, H. (2023). Insights into geospatial
713 heterogeneity of landslide susceptibility based on the SHAP-XGBoost model. Journal of
714 Environmental Management, 332, 117357. https://doi.org/10.1016/j.jenvman.2023.117357

https://doi.org/10.5194/egusphere-2025-2843
Preprint. Discussion started: 28 July 2025

715 Chen, Tianqi & Guestrin, Carlos. (2016). XGBoost: A Scalable Tree Boosting System. 785-794.
716 10.1145/2939672.2939785.
717 Medici, G., West, L. J., & Banwart, S. A. (2019). Groundwater flow velocities in a fractured
718 carbonate aquifer-type: Implications for contaminant transport. Journal of Contaminant Hydrology,
719 222, 1-16. https://doi.org/10.1016/j.jconhyd.2019.02.001
720 Zhang, J., Wang, S., Fu, Z., Wang, K., & Chen, H. (2024). Characterizing rapid infiltration processes
721 on complex hillslopes: Insights from soil moisture response to rainfall events. Journal of Hydrology,
722 644, 132110. https://doi.org/10.1016/j.jhydrol.2024.132110
723 Reimann, T., T. Geyer, W. B. Shoemaker, R. Liedl, and M. Sauter (2011), Effects of dynamically
724 variable saturation and matrix-conduit coupling of flow in karst aquifers, *Water Resour. Res.*, 47,
725 W11503, doi:10.1029/2011WR010446.
726 Reimann, T., T. Geyer, W. B. Shoemaker, R. Liedl, and M. Sauter (2011), Effects of dynamically
727 variable saturation and matrix-conduit coupling of flow in karst aquifers, *Water Resour. Res.*, 47,
728 W11503, doi:10.1029/2011WR010446.
729 Bailly-Comte, V., Martin, J. B., Jourde, H., Screaton, E. J., Pistre, S., & Langston, A. (2010). Water
730 exchange and pressure transfer between conduits and matrix and their influence on hydrodynamics
731 of two karst aquifers with sinking streams. Journal of Hydrology, 386(1-4), 55-66.
732 https://doi.org/10.1016/j.jhydrol.2010.03.005
733 Evans, G. V. (1983). Tracer techniques in hydrology. The International Journal of Applied Radiation
734 and Isotopes, 34(1), 451-475. https://doi.org/10.1016/0020-708X(83)90144-8
735 Ronayne, M. J. (2013). Influence of conduit network geometry on solute transport in karst aquifers
736 with a permeable matrix. Advances in Water Resources, 56, 27-34.
737 https://doi.org/10.1016/j.advwatres.2013.03.002
738 Zhang, J., Wang, S., Fu, Z., Chen, H., & Wang, K. (2022). Soil thickness controls the rainfall-runoff
739 relationship at the karst hillslope critical zone in southwest China. Journal of Hydrology, 609,
740 127779. https://doi.org/10.1016/j.jhydrol.2022.127779
741 Cusano, D., Allocca, V., Coda, S., Di Clemente, E., Fabbrocino, S., Lepore, D., Panza, R., Petrone,
742 P., & De Vita, P. (2024). Effects of ash-fall pyroclastic soil mantle on groundwater recharge of
743 Terminio Mt. peri-volcanic karst aquifer. Journal of Hydrology: Regional Studies, 53, 101844.
744 https://doi.org/10.1016/j.ejrh.2024.101844
745 Anker Y, Gimburg A, Zilberbrand M, Livshitz Y, Mirlas V. Groundwater Recharge Assessment for
746 Small karstic Catchment Basins with Different Extents of Anthropogenic
747 Development. *Environments*. 2023; 10(9):158. https://doi.org/10.3390/environments10090158
748 LI Zhenhua，LI Songtao，DU Feng，*et al*. Research on the development law of karst caves on
749 water conducting fractures under the influence of mining in Southwest karst Mining Areas[J]. Coal
750 Science and Technology，2023，51（7）：106−117. DOI: 10.13199/j.cnki.cst.2023-0409
751 Jiang, Z., Liu, H., Wang, H. *et al.* Bedrock geochemistry influences vegetation growth by regulating
752 the regolith water holding capacity. *Nat Commun* **11**, 2392 (2020). https://doi.org/10.1038/s41467-
753 020-16156-1
754 Wang, F., Chen, H., Lian, J., Fu, Z., & Nie, Y. (2020). Hydrological response of karst stream to
755 precipitation variation recognized through the quantitative separation of runoff components. Science
756 of The Total Environment, 748, 142483. https://doi.org/10.1016/j.scitotenv.2020.142483
757 Wetzel, P. J., Liang, X., Irannejad, P., Boone, A., Noilhan, J., Shao, Y., Skelly, C., Xue, Y., & Yang,
758 Z. L. (1996). Modeling vadose zone liquid water fluxes: Infiltration, runoff, drainage,

https://doi.org/10.5194/egusphere-2025-2843
Preprint. Discussion started: 28 July 2025

interflow. *Global and Planetary Change*, *13*(1–4), 57–71. https://doi.org/10.1016/0921-8181(95)00037-2

Duringer, P., Bacon, A.-M., Sayavongkhamdy, T., & Nguyen, T. K. T. (2012). karst development, breccias history, and mammalian assemblages in Southeast Asia: A brief review. Comptes Rendus Palevol, 11(2–3), 133-157. https://doi.org/10.1016/j.crpv.2011.07.003

Jiang, Z., Liu, H., Wang, H. *et al.* Bedrock geochemistry influences vegetation growth by regulating the regolith water holding capacity. *Nat Commun* **11**, 2392 (2020). https://doi.org/10.1038/s41467-020-16156-1

Teixeira, G. M., de Paula, R. S., Velasquez, L. N. M., Andrade, I. B., & Neto, W. M. P. (2023). Evaluation of recharge estimation methods applied to fissure and karst aquifers of the Lagoa Santa karst Environmental Protection Area, Brazil. *Hydrological Processes*, 37(8), e14971. https://doi.org/10.1002/hyp.14971

Klimchouk, Alexander Borisovich, "Hypogene speleogenesis: Hydrogeological and Morphogenetic Perspective NCKRI - Special Paper 1" (2007). *KIP Monographs*. 13.https://digitalcommons.usf.edu/kip_monographs/13

Jiang, G., Chen, Z., Siripornpibul, C. *et al.* The karst water environment in Southeast Asia: characteristics, challenges, and approaches. *Hydrogeol J* **29**, 123–135 (2021). https://doi.org/10.1007/s10040-020-02267-y

Li, Y., Wang, S., Peng, T., Zhao, G., & Dai, B. (2023). Hydrological characteristics and available water storage of typical karst soil in SW China under different soil–rock structures. Geoderma, 438, 116633. https://doi.org/10.1016/j.geoderma.2023.116633

Goldscheider, Nico. (2015). Overview of Methods Applied in karst Hydrogeology. 10.1007/978-3-319-12850-4_4.

Tapiador, F. J., Turk, F. J., Petersen, W., Hou, A. Y., García-Ortega, E., Machado, L. A. T., … Huffman, G. J. (2012). Global precipitation measurement: Methods, datasets and applications. Atmospheric Research, 104–105, 70-97. https://doi.org/10.1016/j.atmosres.2011.10.021

Wang, S., Yan, Y., Zhao, Y., Fu, Z., & Chen, H. (2024). Co-evolution among soil thickness, epikarst weathering degree, and runoff characteristics on a subtropical karst hillslope. *Journal of Hydrology, 628*, 130499. https://doi.org/10.1016/j.jhydrol.2023.130499

Fu, Z., Chen, H., Xu, Q., Jia, J., Wang, S., and Wang, K. (2016) Role of epikarst in near-surface hydrological processes in a soil mantled subtropical dolomite karst slope: implications of field rainfall simulation experiments. Hydrol. Process., 30: 795–811. doi: 10.1002/hyp.10650.

Liu, X., Fu, Z., Zhang, W., Xiao, S., Chen, H., & Wang, K. (2023). Soluble carbon loss through multiple runoff components in the shallow subsurface of a karst hillslope: Impact of critical zone structure and land use. *CATENA, 222*, 106868. https://doi.org/10.1016/j.catena.2022.106868

Jasechko, S., Seybold, H., Perrone, D. *et al.* Rapid groundwater decline and some cases of recovery in aquifers globally. *Nature* 625, 715–721 (2024). https://doi.org/10.1038/s41586-023-06879-8

de Graaf, I.E.M., Gleeson, T., (Rens) van Beek, L.P.H. *et al.* Environmental flow limits to global groundwater pumping. *Nature* 574, 90–94 (2019). https://doi.org/10.1038/s41586-019-1594-4

Liu, B., Chen, C., Lian, Y., Chen, J., & Chen, X. (2015). Long-term change of wet and dry climatic conditions in the southwest karst area of China. *Global and Planetary Change*, *127*, 1-11. https://doi.org/10.1016/j.gloplacha.2015.01.009

Hartmann, A., Goldscheider, N., Wagener, T., Lange, J., & Weiler, M. (2014). karst water resources

https://doi.org/10.5194/egusphere-2025-2843
Preprint. Discussion started: 28 July 2025

in a changing world: Review of hydrological modeling approaches. *Reviews of Geophysics*, *52*(3), 218-242. https://doi.org/10.1002/2013RG000443

D'Ettorre, U. S., Liso, I. S., & Parise, M. (2024). Desertification in karst areas: A review. Earth-Science Reviews, 253, 104786. https://doi.org/10.1016/j.earscirev.2024.104786

Kang T, Lee S, Lee N, Jin Y. Baseflow Separation Using the Digital Filter Method: Review and Sensitivity Analysis. *Water*. 2022; 14(3):485. https://doi.org/10.3390/w14030485

Rattayová, V., & Hlavčová, K. (2023). Base flow separation method in conditions of the karst catchment. *Pollack Periodica*, *18*(2), 72-77.

Helfer, F., Bernardi, F. K., Barros, C. A. P. de, Piccilli, D. G. A., Minella, J. P. G., Tassi, R., & Schlesner, A. A. (2024). Calibrated Eckhardt's filter versus alternative baseflow separation methods: A silica-based approach in a Brazilian catchment. Journal of Hydrology, 644, 132073. https://doi.org/10.1016/j.jhydrol.2024.132073

Zhou, X., Shen, C., Ni, G., & Hu, H. (2017). Digital filter-based baseflow separation method combined with recession curves. Journal of Tsinghua University, 57(03), 318-330. https://doi.org/10.16511/j.cnki.qhdxxb.2017.26.016

Lebakula V , Sims K , Reith A ,et al.LandScan Global 30 Arcsecond Annual Global Gridded Population Datasets from 2000 to 2022. Scientific Data, 2025, 12(1).DOI:10.1038/s41597-025-04817-z.

Author contributions

Ze Yuan: Conceptualization, Methodology, Writing – original draft.
Qiuwen Zhou: Formal analysis, Investigation, Writing – review & editing.
Yuan Li: Data curation, Visualization, Software.
Yuluan Zhao: Validation, Resources, Project administration.
Shengtian Yang: Supervision, Funding acquisition, Writing – review & editing.

Acknowledgments

The authors thank all those who provided valuable assistance during the experimental process.